

Minerva Access is the Institutional Repository of The University of Melbourne

Author/s:

Catani, KJ;Sanelli, JA;Dryza, V;Gilka, N;Taylor, PR;Bieske, EJ

Title:

Electronic spectrum of the propargyl cation ($\text{H}_2\text{C}_3\text{H}^+$) tagged with Ne and N_2

Date:

2015-11-14

Citation:

Catani, K. J., Sanelli, J. A., Dryza, V., Gilka, N., Taylor, P. R. & Bieske, E. J. (2015). Electronic spectrum of the propargyl cation ($\text{H}_2\text{C}_3\text{H}^+$) tagged with Ne and N_2 . *Journal of Chemical Physics*, 143 (18), <https://doi.org/10.1063/1.4935169>.

Persistent Link:

<https://hdl.handle.net/11343/58277>

1 **Electronic spectrum of the propargyl cation ($\text{H}_2\text{C}_3\text{H}^+$) tagged with Ne and N_2**

2 Katherine J. Catani,¹ Julian A. Sanelli,¹ Viktoras Dryza,¹ Natalie Gilka,² Peter R.
3 Taylor,^{1, a)} and Evan J. Bieske^{1, b)}

4 ¹⁾*School of Chemistry, The University of Melbourne, Victoria,*
5 *Australia 3010*

6 ²⁾*School of Mathematics and Statistics, The University of Melbourne, Victoria,*
7 *Australia 3010*

8 (Dated: 1 January 2016)

The $\tilde{A}^1A_1 \leftarrow \tilde{X}^1A_1$ band system of the propargyl cation ($\text{H}_2\text{C}_3\text{H}^+$) is measured over the 230-270 nm range by photodissociation of mass-selected $\text{H}_2\text{C}_3\text{H}^+$ -Ne and $\text{H}_2\text{C}_3\text{H}^+$ - N_2 complexes in a tandem mass spectrometer. The band origin occurs at $37\,618\text{ cm}^{-1}$ for $\text{H}_2\text{C}_3\text{H}^+$ -Ne and $37\,703\text{ cm}^{-1}$ for $\text{H}_2\text{C}_3\text{H}^+$ - N_2 . Ground and excited state *ab initio* calculations for $\text{H}_2\text{C}_3\text{H}^+$ using the MCSCF and CC response methods show that the ion has C_{2v} symmetry in the ground \tilde{X}^1A_1 and excited \tilde{A}^1A_1 states and that the strong vibronic progression, with a spacing of 630 cm^{-1} is due to the C-C stretch vibrational mode, ν_5 .

^{a)}Electronic mail: prtaylor@unimelb.edu.au

^{b)}Electronic mail: evanj@unimelb.edu.au

9 I. INTRODUCTION

10 Although small hydrocarbon cations play important roles in combustion, plasmas and
 11 interstellar space, many are yet to be fully characterized from a spectroscopic standpoint.
 12 This is the case for the $C_3H_3^+$ ion, which, as shown in Fig. 1, has two energetically viable
 13 isomers, the cyclopropenyl cation ($c-C_3H_3^+$) and the propargyl cation ($H_2C_3H^+$). The $c-$
 14 $C_3H_3^+$ cation (D_{3h} symmetry) is the lower energy form and is the smallest aromatic system,
 15 with two π -electrons delocalized over the carbon framework. The $H_2C_3H^+$ cation (C_{2v} sym-
 16 metry) lies 105 kJ/mol higher in energy and is more reactive than its cyclic counterpart.^{1,2}
 17 Both isomers are commonly observed fragments in mass spectroscopy and can be distin-
 18 guished by a difference in reactivities.² Furthermore, $c-C_3H_3^+$ and $H_2C_3H^+$ are considered
 19 to be important intermediates in combustion chemistry, playing a role in soot formation.³
 20 The two ions are also postulated to be present in the interstellar medium (ISM) and in
 21 planetary atmospheres.⁴ The extraterrestrial presence of $C_3H_3^+$ has been confirmed by mass
 22 spectrometric observations of ions in the tail of the comet Halley.⁵ $H_2C_3H^+$ and $c-C_3H_3^+$ are
 23 also predicted to play roles in the synthesis of cumulenenic and cyclic C_3H_2 , which are sus-
 24 pected to exist in large abundance in dark and diffuse clouds of the ISM.^{6,7}

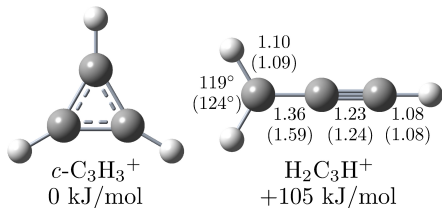


FIG. 1. The $c-C_3H_3^+$ and $H_2C_3H^+$ isomers. For $H_2C_3H^+$, calculated ground and excited state structural parameters are shown (bond lengths in Å, excited state parameters in parenthesis).

25 Due to its widespread relevance the propargyl cation has been the subject of theo-
 26 retical investigations,⁸⁻¹¹ photoelectron studies,^{12,13} IR spectroscopy,¹⁴⁻¹⁷ and electronic
 27 spectroscopy.¹⁶ Information on the ground state vibrational frequencies of $H_2C_3H^+$ has been
 28 derived from photoelectron spectra of H_2C_3H and through infrared photodissociation spec-
 29 tra of $H_2C_3H^+$ cations tagged with Ne, Ar, N_2 , O_2 and CO_2 .^{9,14,15,17} These photodissociation
 30 spectra are congested and difficult to interpret in the CH stretch region due to the presence
 31 of both $H_2C_3H^+$ and $c-C_3H_3^+$ species and various isomers associated with the tag atom or
 32 molecule attached at different sites, and also by the occurrence of overtone and combinations

33 bands.

34 The $\tilde{A}^1A_1 \leftarrow \tilde{X}^1A_1$ electronic band system of $\text{H}_2\text{C}_3\text{H}^+$ in a Ne matrix was first measured
35 by Wyss *et al.*¹⁶ The band system, extending from 268 down to 240 nm, displayed a strong
36 vibronic progression that was assigned to a CCH bending vibrational mode, implying a
37 reduction of symmetry from the C_{2v} ground state to a C_s excited state. The observed bands
38 were relatively broad, possibly concealing weaker transitions.

39 To further characterize the $\text{H}_2\text{C}_3\text{H}^+$ molecular cation we have measured the $\tilde{A}^1A_1 \leftarrow \tilde{X}^1A_1$
40 electronic spectra over the 235-270 nm range of the $\text{H}_2\text{C}_3\text{H}^+$ -Ne and $\text{H}_2\text{C}_3\text{H}^+$ -N₂ complexes
41 by photodissociating them in a tandem mass spectrometer. The new photodissociation spec-
42 tra exhibit more clearly resolved bands than the previous Ne matrix spectrum, providing a
43 better view of the dominant progression, and allowing several new transitions to be observed.
44 Complementary electronic structure calculations are conducted to provide structural param-
45 eters for $\text{H}_2\text{C}_3\text{H}^+$ in the ground and excited states and to assist in interpreting the measured
46 spectra. An important aspect of the work is consideration of whether the extended vibronic
47 progression in the $\tilde{A}^1A_1 \leftarrow \tilde{X}^1A_1$ electronic transition is indeed associated with a linear-bent
48 transition accompanying a reduction in molecular symmetry from C_{2v} to C_s .

49 II. EXPERIMENTAL METHODS

50 The electronic spectrum of $\text{H}_2\text{C}_3\text{H}^+$ was recorded by resonance-enhanced photodisso-
51 ciation of the $\text{H}_2\text{C}_3\text{H}^+$ -Ne and $\text{H}_2\text{C}_3\text{H}^+$ -N₂ complexes in a tandem mass spectrometer,
52 in each case by monitoring $\text{H}_2\text{C}_3\text{H}^+$ photofragments. The equipment has been described
53 previously,¹⁸⁻²¹ and here we provide only a brief outline. Vapour from a solution of propargyl
54 bromide ($\text{C}_3\text{H}_3\text{Br}$) in toluene, cooled to 0°C, was seeded into a pulsed supersonic expansion
55 of nitrogen or neon gas (backing pressure 4 bar) and bombarded with electrons to form
56 the $\text{H}_2\text{C}_3\text{H}^+$ closed-shell cation. $\text{H}_2\text{C}_3\text{H}^+$ -Ne or $\text{H}_2\text{C}_3\text{H}^+$ -N₂ were formed through 3-body
57 collisions in the free-jet expansion and mass-selected by a quadrupole mass filter. Charged
58 complexes were then deflected 90° by an electrostatic quadrupole bender into an octopole
59 ion guide and irradiated with light from a tuneable optical parametric oscillator (OPO,
60 EKSPLA NT342B) with a bandwidth of $\approx 8\text{ cm}^{-1}$. Resonant photoexcitation of $\text{H}_2\text{C}_3\text{H}^+$ -
61 Ne or $\text{H}_2\text{C}_3\text{H}^+$ -N₂ generated $\text{H}_2\text{C}_3\text{H}^+$ photofragments that were mass-selected by a second
62 quadrupole mass filter and detected by a microchannel plate. The $\text{H}_2\text{C}_3\text{H}^+$ ion signal was

63 monitored as the laser wavelength was scanned to record a photodissociation action spec-
64 trum, that was subsequently normalized with respect to laser power. Wavelength calibration
65 was performed using a wavemeter (Ångstrom LSA UVL).

66 Note that we did not target the $C_3H_3^+$ -Ar complex because of its near mass coincidence
67 with the extremely abundant Ar_2^+ cation. Furthermore, we were unable to detect photodis-
68 sociation of the untagged $C_3H_3^+$ cation.

69 There are several different possible photodissociation mechanisms. For example, electron-
70 ically excited $H_2C_3H^+$ -Ne or $H_2C_3H^+$ - N_2 may undergo non-radiative decay to the ground
71 state manifold, leading to rapid fragmentation of the vibrationally energized complex. It
72 is also plausible that the complexes dissociate following fluorescence to excited vibrational
73 levels in the ground state manifold lying above the dissociation threshold ($D_e=241$ and
74 1435 cm^{-1} for $H_2C_3H^+$ -Ne and $H_2C_3H^+$ - N_2 , respectively⁹).

75 III. COMPUTATIONAL METHODS

76 The $H_2C_3H^+$ cation was examined computationally using several different approaches
77 to determine ground and excited state structures and vibrational frequencies. Ground-
78 and excited-state geometries and vibrational frequencies were calculated at the restricted
79 active space self-consistent field (RASSCF)²² level of theory using a cc-pVTZ basis set.
80 State-averaging was not used: the ground- and excited-state wave functions were optimized
81 in independent calculations as respectively the first and second roots of symmetry 1A_1 .
82 The active orbital space of 15 MOs (the three C 1s-derived MOs were held inactive) was
83 partitioned as follows. The RAS1 space comprised four MOs of a_1 symmetry and one in b_2 ,
84 the RAS2 space two in b_1 and two in b_2 , and the RAS3 space four in a_1 , and one each in b_1
85 and b_2 . In essence, the RAS1 space described the σ -bonding orbitals, the RAS2 space the
86 “in-plane” and out of plane π -bonding and antibonding orbitals, and the RAS3 space the
87 remaining valence MOs. The RAS1 space was constrained to contain at least eight electrons,
88 and the RAS3 space at most two. Compared to a full CASSCF calculation the RASSCF
89 configuration space comprises some 7 000 configurations as opposed to well over 2 300 000:
90 comparisons in a smaller atomic basis indicate that the difference in the calculated results
91 is almost negligible. This RASSCF approach should give a balanced treatment of both
92 states, but will necessarily suffer from the lack of dynamical correlation. In an attempt to

93 improve on these results we have performed CC3 linear response (CC3LR) calculations, in
94 the cc-pVQZ basis, of the excitation energy, and have re-optimized the ground- and excited-
95 state geometries using the CCSDT and EOM-CCSDT (CCSDT linear response, in effect)
96 methods respectively, again in the cc-pVTZ basis. This should give a better estimate of the
97 geometries — it is unfortunately not feasible to recompute the vibrational frequencies at
98 this level.

99 The Dalton program²³ was used for the CASSCF and CC3/CC3LR energy calculations,
100 and the CCSDT/EOM-CCSDT geometry optimizations were performed using CFOUR.²⁴
101 Vibrational modes were classified by their symmetries in the C_{2v} point group and numbered
102 according to the Mulliken convention.²⁵

103 The isomers of $H_2C_3H^+$ -Ne and $H_2C_3H^+$ -N₂ were characterized computationally by
104 Botschwina and coworkers at the CCSD(T*)-F12a level giving relative energies and struc-
105 tures. However vibrational frequencies for the intermolecular modes were not reported.
106 Therefore, the structures and vibrational frequencies of $H_2C_3H^+$ -Ne and $H_2C_3H^+$ -N₂ com-
107 plexes were examined employing density functional theory (DFT) with the ω B97X-D
108 functional²⁶ and aug-cc-pVTZ basis set. This level of theory, which incorporates empir-
109 ical dispersion corrections, has been used for other charged non-covalently bound systems
110 including quinoline⁺-Ar and isoquinoline⁺-Ar,²⁰ indene⁺-Ar,²¹ and indole⁺-Ar.²⁷ These cal-
111 culations were performed with the Gaussian 09 program suite.²⁸ Calculated vibrational
112 frequencies of the complexes are provided in the supplemental material.²⁹

113 IV. RESULTS AND DISCUSSION

114 A. Ground and excited state geometries, frequencies and excitation energies 115 for $H_2C_3H^+$

116 The RASSCF/cc-pVTZ ground and excited state geometrical parameters for $H_2C_3H^+$ are
117 shown in Fig. 1. Ground state structural parameters are very similar to those found through
118 DFT/B3LYP/cc-pVTZ calculations by Ricks *et al.*¹⁵ and the CCSD(T*)-F12a calculations
119 by Botschwina *et al.*⁸

120 The predicted structural effects of exciting $H_2C_3H^+$ to the \tilde{A}^1A_1 state are summarized
121 in Table I. The change in the first C–C bond length is particularly noteworthy. The excited

122 state wave function is dominated by excitation from the bonding π orbital to its antibond-
 123 ing counterpart and this substantially weakens the first C–C bond. Incidentally, the wave
 124 function contains significant contribution from the *double* excitation $\pi^2 \rightarrow \pi^{*2}$ as well as the
 125 corresponding single excitation, making it clear that this excited state is a poor candidate
 126 for single configuration-based methods such as LR-DFT. As expected, the weaker π bond
 127 results in a change in the angles around the methylene carbon, with the HCH angle opening
 128 by 5° . The calculated harmonic frequencies largely reflect expectations from the geometry
 129 changes from ground to excited state: modes expected to be largely unaffected by the weak-
 130 ening of the π bond have similar values between ground and excited state, whereas the C–C
 131 stretching frequency is predicted to decrease by over 400 cm^{-1} , and the C \equiv C stretch by
 132 200 cm^{-1} , for example.

TABLE I. Differences between ground and excited state geometries at the RASSCF/cc-pVTZ and the CCSDT/EOM-CCSDT level. Bond lengths in Å and angles in degrees.

	Δ RASSCF	Δ CCSDT
r(C–C)	0.227	0.188
r(C \equiv C)	0.005	0.009
r(CH) (CH ₂)	–0.006	–0.002
r(CH) (CH)	–0.002	–0.002
\angle HCH	5.4	3.7

133 Improved geometry estimates from CCSDT calculations suggest that the increase in the
 134 C–C bond length as a result of excitation is somewhat overestimated by RASSCF: the latter
 135 suggests almost 0.23 Å increase whereas the CCSDT/EOM-CCSDT results suggest a smaller
 136 increase of 0.19 Å . This overestimation of the bond length change by RASSCF undoubtedly
 137 accounts for some of the discrepancies between the observed Franck-Condon profiles and
 138 those obtained by simulating the spectra as shown in the supplemental material.²⁹ Differences
 139 between the RASSCF and CCSDT/EOM-CCSDT results for the other geometry parameters
 140 are negligible at this level of accuracy.

141 At the CC3/CC3LR level, using the RASSCF-optimized geometries, the adiabatic T_e
 142 excitation energy is predicted to be $38\,800 \text{ cm}^{-1}$, and using the RASSCF estimates for the
 143 zero-point vibrational contribution yields a T_0 value of $38\,100 \text{ cm}^{-1}$. The vertical excitation

144 energy at the ground-state RASSCF geometry is predicted to be $41\,100\text{ cm}^{-1}$. We note that
 145 these predictions are for the isolated $\text{H}_2\text{C}_3\text{H}^+$ molecule, but the effect of the tethered species
 146 on the excitation energy is expected to be minor and thus these results should be directly
 147 relevant to the analysis of experiment here. Agreement appears to be within 1000 cm^{-1} ,
 148 which is as good or better than would be expected for these methods.

TABLE II. Calculated harmonic vibrational frequencies for $\text{H}_2\text{C}_3\text{H}^+$ compared to experimental frequencies derived from spectra of $\text{H}_2\text{C}_3\text{H}^+\text{-Ar}$, $\text{H}_2\text{C}_3\text{H}^+\text{-Ne}$ and $\text{H}_2\text{C}_3\text{H}^+\text{-N}_2$.

Mode	Description	\tilde{X}^1A_1		\tilde{A}^1A_1		
		Calc. ^a	Exp.	Calc. ^a	Exp.	Exp.
				$\text{H}_2\text{C}_3\text{H}^+\text{-N}_2^d$		$\text{H}_2\text{C}_3\text{H}^+\text{-Ne}^d$
$\nu_1(a_1)$	C–H stretch	3320	3238 ^b	3338		
$\nu_2(a_1)$	CH ₂ sym. stretch	3072	3004 ^b	3102	2897*	2912*
$\nu_3(a_1)$	C≡C stretch	2116	2077 ^b	1893		
$\nu_4(a_1)$	CH ₂ scissors	1500	1445 ^b	1416		1346
$\nu_5(a_1)$	C–C stretch	1125	1122 ^b	685	628	629
$\nu_6(b_1)$	CH ₂ out-of-plane wag	1142	1111 ^b	722		
$\nu_7(b_1)$	CCH out-of-plane bend	873	858 ^c	514		
$\nu_8(b_1)$	CCC out-of-plane bend	268		263		
$\nu_9(b_2)$	CH ₂ antisym. stretch	3171	3093 ^b	3250		
$\nu_{10}(b_2)$	CH ₂ in-plane wag	1059		998		
$\nu_{11}(b_2)$	CCH in-plane bend	627		680		
$\nu_{12}(b_2)$	CCC in-plane bend	283		245		

*tentative assignment

^a RASSCF/cc-pVTZ calculations (unscaled)

^b from IRPD spectrum of $\text{H}_2\text{C}_3\text{H}^+\text{-Ar}$ (ref. 15)

^c from photoelectron data (ref. 13)

^d this work

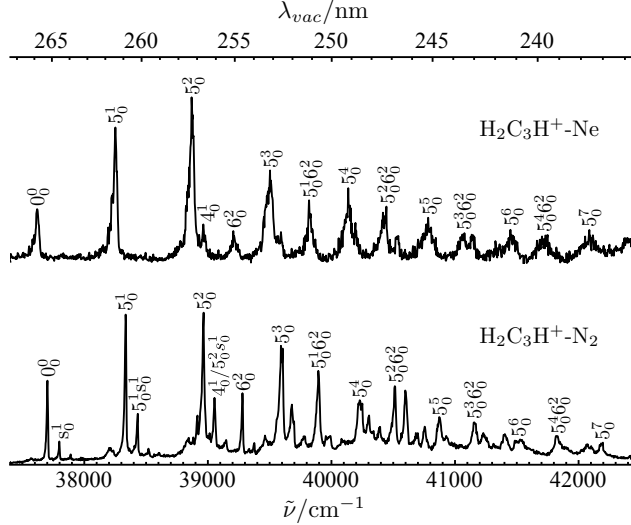


FIG. 2. The $\tilde{A}^1A_1 \leftarrow \tilde{X}^1A_1$ band system of $\text{H}_2\text{C}_3\text{H}^+\text{-Ne}$ (top) and $\text{H}_2\text{C}_3\text{H}^+\text{-N}_2$ (bottom), recorded by monitoring $\text{H}_2\text{C}_3\text{H}^+$ photofragments as a function of laser wavelength.

149 B. Electronic spectra of $\text{H}_2\text{C}_3\text{H}^+\text{-Ne}$ and $\text{H}_2\text{C}_3\text{H}^+\text{-N}_2$

150 The $\tilde{A}^1A_1 \leftarrow \tilde{X}^1A_1$ electronic spectra of $\text{H}_2\text{C}_3\text{H}^+\text{-Ne}$ and $\text{H}_2\text{C}_3\text{H}^+\text{-N}_2$ over the 230–270 nm
 151 range are shown in Fig. 2. Measured peak positions are compiled in Table III, while fully
 152 assigned spectra are included in the SI. As observed by Wyss *et al.* for $\text{H}_2\text{C}_3\text{H}^+$ in a Ne
 153 matrix,¹⁶ the $\tilde{A}^1A_1 \leftarrow \tilde{X}^1A_1$ band system is dominated by an extended progression with a
 154 spacing of $\approx 630 \text{ cm}^{-1}$. The $\text{H}_2\text{C}_3\text{H}^+\text{-N}_2$ and $\text{H}_2\text{C}_3\text{H}^+\text{-Ne}$ spectra are very similar, although
 155 peaks in the $\text{H}_2\text{C}_3\text{H}^+\text{-N}_2$ spectrum are sharper and shifted to higher energy than their
 156 $\text{H}_2\text{C}_3\text{H}^+\text{-Ne}$ counterparts. As well, the $\text{H}_2\text{C}_3\text{H}^+\text{-N}_2$ spectrum includes additional bands due
 157 to excitation of intermolecular modes, presumably the intermolecular stretch mode (ν_s).
 158 These transitions are discussed in Section IV E below. The origin transition for $\text{H}_2\text{C}_3\text{H}^+\text{-Ne}$
 159 occurs at $37\,618 \pm 15 \text{ cm}^{-1}$, whereas the origin band for $\text{H}_2\text{C}_3\text{H}^+\text{-N}_2$ lies at $37\,703 \pm 15 \text{ cm}^{-1}$,
 160 85 cm^{-1} to higher energy. It is worth noting that the band origin for $\text{H}_2\text{C}_3\text{H}^+$ in a Ne matrix
 161 is shifted by 288 cm^{-1} to lower energy with respect to the origin of the $\text{H}_2\text{C}_3\text{H}^+\text{-Ne}$ complex.

162 C. Main band assignments

163 The $\text{H}_2\text{C}_3\text{H}^+\text{-Ne}$ and $\text{H}_2\text{C}_3\text{H}^+\text{-N}_2$ spectra are dominated by a single progression extending
 164 for at least 6 quanta. Previously, Wyss *et al.* argued that the main progression was due to

165 the ν_{11} CCH in-plane bending mode, that becomes Franck-Condon active in a distorted C_s
 166 excited \tilde{A}^1A_1 state.¹⁶ Our RASSCF/cc-pVTZ calculations indicate that $H_2C_3H^+$ retains C_{2v}
 167 symmetry in the \tilde{A}^1A_1 state and that the progression arises from ν_5 , primarily a C-C stretch
 168 vibration that drops in frequency from 1125 to 685 cm^{-1} upon electronic excitation with a
 169 concomitant increase in the C-C bond length (accounting for the extended 5_0^n progression).

170 Simulation of the spectrum using the RASSCF/cc-pVTZ geometrical parameters (Fig.1)
 171 and vibrational frequencies (Table II) supports assignment of the dominant progression to ν_5 ,
 172 although the length of the progression is overestimated with a better match to experiment
 173 being given for a 0.16 Å elongation of the C-C bond rather than the CCSDT/EOM-CCSDT
 174 value of 0.19 Å. Simulated spectra for a range of bond length changes are provided in the
 175 supplemental material.²⁹ Note that the assignment of the dominant progression to the ν_5 CC
 176 stretch vibrational mode is consistent with Wyss *et al.*'s observation of only a small reduc-
 177 tion in the progression spacing following deuteration (667 cm^{-1} for $H_2C_3H^+$ and 641 cm^{-1} for
 178 $D_2C_3D^+$).¹⁶

179 Aside from the dominant ν_5 progression, several weaker transitions also appear in the
 180 $H_2C_3H^+-Ne$ and $H_2C_3H^+-N_2$ spectra. For $H_2C_3H^+-Ne$, a transition appears at 0_0^0+1346 cm^{-1} that
 181 can be assigned to the 4_0^1 transition (CH_2 symmetric bend mode), which has a calculated
 182 excited state frequency of 1416 cm^{-1} . Higher $4_0^15_0^n$ transitions eventually merge with the
 183 5_0^{n+2} bands. The corresponding $4_0^15_0^n$ transitions of $H_2C_3H^+-N_2$ overlap with transitions
 184 involving the intermolecular stretch mode ($5_0^{n+2}s_0^1$) and are difficult to resolve.

185 Another prominent transition occurs at 0_0^0+1585 cm^{-1} for $H_2C_3H^+-Ne$ and 0_0^0+1576 cm^{-1} for
 186 $H_2C_3H^+-N_2$, approximately midway between the 5_0^2 and 5_0^3 transitions. Assignment of this
 187 band is uncertain. The only possible mode of a_1 symmetry is ν_3 ($C\equiv C$ acetylenic stretch),
 188 which has a calculated excited state frequency of 1893 cm^{-1} , 315 cm^{-1} or 20% higher than
 189 the observed spacing, making it unlikely that it is responsible for the band. Alternatively,
 190 the 0_0^0+1585 cm^{-1} transition may correspond to two quanta of a vibrational mode with b_1 or
 191 b_2 symmetry and with a frequency of ≈ 790 cm^{-1} . On the basis of the calculated frequencies,
 192 the most likely mode is the ν_6 (b_1) CH_2 out-of-plane wag. As well, the substantial reduction
 193 in ν_6 frequency between the \tilde{X} and \tilde{A} states (from 1142 to 722 cm^{-1}), means that the 6_0^2
 194 transition has appreciable intensity. This assignment implies that the RASSCF/cc-pVTZ
 195 ν_6 frequency underestimates the actual value by around 10%, suggesting that ν_6 possesses
 196 substantial negative anharmonicity, or that this mode is substantially affected by dynamical

197 correlation effects not captured by methods like RASSCF or CASSCF.

198 Evidence for the activity of other a_1 vibrational modes (*eg.* the ν_1 acetylenic and ν_2
199 methylenic C-H stretches) is equivocal. A peak appearing at $0_0^0+2912\text{ cm}^{-1}$ for $\text{H}_2\text{C}_3\text{H}^+\text{-Ne}$
200 and $0_0^0+2897\text{ cm}^{-1}$ for $\text{H}_2\text{C}_3\text{H}^+\text{-N}_2$ can tentatively be assigned to the 2_0^1 transition (CH_2
201 symmetric stretch), while a band assignable to the $2_0^15_0^1$ transition is also observed for both
202 molecules. These assignments imply a ν_2 frequency $\approx 200\text{ cm}^{-1}$ lower than the calculated
203 excited state value (3102 cm^{-1}).

204 D. $\text{H}_2\text{C}_3\text{H}^+\text{-Ne}$ spectrum

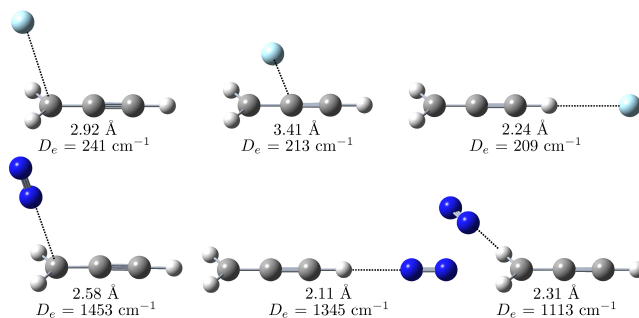


FIG. 3. Most stable structures for $\text{H}_2\text{C}_3\text{H}^+\text{-Ne}$ (top) and $\text{H}_2\text{C}_3\text{H}^+\text{-N}_2$ (bottom). Dissociation energies (D_e) and intermolecular distances calculated at the CCSD(T*)-F12a level (from ref. 9) are indicated for each structure.

205 Having considered the main features of the $\text{H}_2\text{C}_3\text{H}^+$ electronic spectrum we turn now to a
206 brief discussion of the properties of the $\text{H}_2\text{C}_3\text{H}^+\text{-Ne}$ and $\text{H}_2\text{C}_3\text{H}^+\text{-N}_2$ species. The best guide
207 to the structures and energetics of the two complexes comes from the CCSD(T*)-F12a level
208 calculations by Botschwina *et al.*, who predicted three stable isomers for each species (see
209 Fig. 3).⁹ For the lowest energy $\text{H}_2\text{C}_3\text{H}^+\text{-Ne}$ isomer, the C-bound isomer, the Ne atom resides
210 above the molecular plane, adjacent the methylenic carbon (C_s symmetry, $D_e=241\text{ cm}^{-1}$).
211 Lying slightly higher in energy is the in-plane isomer, with the Ne atom situated in the
212 molecular plane closest to a methylenic hydrogen (C_s symmetry, $D_e=213\text{ cm}^{-1}$). Having a
213 similar energy is an H-bound isomer with the Ne atom lying on the C_2 axis adjacent to the
214 acetylenic hydrogen (C_{2v} symmetry, $D_e=209\text{ cm}^{-1}$). The 3 isomers of $\text{H}_2\text{C}_3\text{H}^+\text{-Ne}$ are shown
215 in Fig. 3.

216 It is not clear which $\text{H}_2\text{C}_3\text{H}^+$ -Ne isomer is responsible for the observed electronic spec-
217 trum. Because only one series of peaks is seen, either there is only a single contributing
218 isomer or the different isomers have similar electronic transition frequencies. Indeed it is
219 conceivable that the asymmetric bands, which are shaded to lower energy, and have widths of
220 $\approx 50\text{ cm}^{-1}$, reflect the overlapping absorptions of isomers with slightly different band shifts.

221 E. $\text{H}_2\text{C}_3\text{H}^+$ - N_2 spectrum

222 According to the calculations of Botschwina *et al.*,⁹ $\text{H}_2\text{C}_3\text{H}^+$ - N_2 has three stable isomers
223 possessing similar structures to the $\text{H}_2\text{C}_3\text{H}^+$ -Ne isomers, but with significantly higher disso-
224 ciation energies (see Fig. 3). The lowest energy C-bound $\text{H}_2\text{C}_3\text{H}^+$ - N_2 isomer (C_s symmetry,
225 $D_e=1453\text{ cm}^{-1}$), H-bound isomer (C_{2v} symmetry, $D_e=1345\text{ cm}^{-1}$), and in-plane isomer (C_s
226 symmetry, $D_e=1113\text{ cm}^{-1}$).⁹ On the basis of measured infrared band intensities Dopfer *et*
227 *al.* estimated a population ratio of 2:1 for C-bound versus H-bound forms of $\text{H}_2\text{C}_3\text{H}^+$ - N_2 ,
228 consistent with their relative binding energies and presence of two C-bound minima (N_2
229 above and below the plane) and only a single H-bound minimum on the $\text{H}_2\text{C}_3\text{H}^+$ + N_2 PES.⁹
230 Most of the features in the $\text{H}_2\text{C}_3\text{H}^+$ - N_2 spectrum shown in Fig. 3 can be convincingly as-
231 signed to a single isomer. However, depending on the backing pressure and distance between
232 the nozzle and electron impact zone, additional peaks appear, shifted to lower energy from
233 the dominant peaks by $\approx 130\text{ cm}^{-1}$. These peaks are presumably associated with a second
234 isomer (see Fig. 4). At this stage we are unsure which of the three isomers is responsible
235 for each set of peaks. Clarification of the peak assignments may be possible through IR-
236 UV hole-burning experiments. If the assignments of Dopfer *et al.* are correct, the H-bound
237 and C-bound forms have ν_1 CH stretch absorptions at 3139 and 3243 cm^{-1} , respectively.⁹
238 Excitation of one of these IR bands should deplete the dominant UV transitions.

239 As mentioned above, the $\text{H}_2\text{C}_3\text{H}^+$ - N_2 spectrum contains weak transitions spaced by $+95$
240 and $+187\text{ cm}^{-1}$ with respect to the main transitions (see Fig. 4) that are absent from the
241 $\text{H}_2\text{C}_3\text{H}^+$ -Ne spectrum, and are most likely due to excitation of intermolecular modes, par-
242 ticularly the intermolecular stretch vibrational mode (ν_s), which according to DFT calcula-
243 tions ($\omega\text{B97XD}/\text{aug-cc-pVTZ}$) has a frequency of 103 cm^{-1} for the linear H-bonded isomer,
244 93 cm^{-1} for the C-bound isomer, and 91 cm^{-1} for the in-plane isomer (see SI). It is also
245 conceivable that the bands are associated with an a' intermolecular bending mode for the

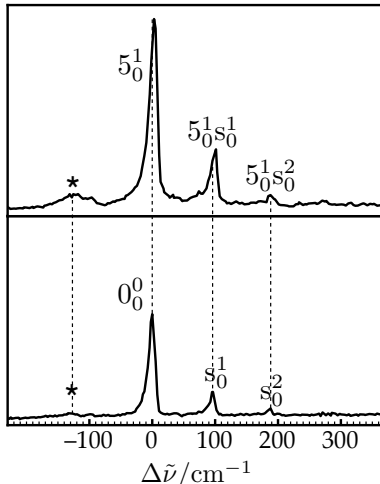


FIG. 4. Expanded view of the 0_0^0 and 5_0^1 peaks of $\text{H}_2\text{C}_3\text{H}^+-\text{N}_2$ showing transitions involving the intermolecular stretch mode (s_0^1 and s_0^2). Transitions assigned to a second isomer are denoted with an asterisk.

246 C-bound $\text{H}_2\text{C}_3\text{H}^+-\text{N}_2$ isomer. For example, the a' intermolecular bending modes of the
 247 C-bound isomer have predicted frequencies of 51 and 133 cm^{-1} , respectively. fgr:spectra

248 It is obvious that the vibronic bands of $\text{H}_2\text{C}_3\text{H}^+-\text{Ne}$ are broader than those of $\text{H}_2\text{C}_3\text{H}^+-$
 249 N_2 (see Fig. 2). As mentioned in the preceding section, the broad asymmetric bands of
 250 $\text{H}_2\text{C}_3\text{H}^+-\text{Ne}$ may reflect overlapping absorptions of several different isomers. It is also possi-
 251 ble that the $\text{H}_2\text{C}_3\text{H}^+-\text{Ne}$ complexes are warm and have quanta in the intermolecular stretch
 252 and bend vibrational modes, and that the observed bands are composed of overlapping hot
 253 bands of the type (s_1^1 , s_2^2 , b_1^1 , b_2^2 etc.) that are progressively displaced to lower frequency due
 254 to a shallower excited state intermolecular potential energy surface. In the case of $\text{H}_2\text{C}_3\text{H}^+-$
 255 N_2 , one might expect that the intermolecular modes will have higher frequencies, so that
 256 the hot bands will be less prominent.

257 V. SUMMARY AND CONCLUSIONS

258 Electronic spectra of the mass-selected $\text{H}_2\text{C}_3\text{H}^+-\text{Ne}$ and $\text{H}_2\text{C}_3\text{H}^+-\text{N}_2$ complexes have been
 259 measured over the 230–270 nm range by monitoring their photodissociation in a tandem mass
 260 spectrometer. A prominent band system is observed corresponding to the $\tilde{A}^1A_1 \leftarrow \tilde{X}^1A_1$ tran-
 261 sition, with an origin at $37\,618 \pm 15\text{ cm}^{-1}$ for $\text{H}_2\text{C}_3\text{H}^+-\text{Ne}$ and $37\,703 \pm 15\text{ cm}^{-1}$ for $\text{H}_2\text{C}_3\text{H}^+-$
 262 N_2 . In both cases, the $\tilde{A}^1A_1 \leftarrow \tilde{X}^1A_1$ band system exhibits well resolved vibronic structure,

263 which is deciphered with the use of electronic structure calculations. The strong Franck-
264 Condon active mode, previously assigned to a CCH in-plane bend mode,¹⁶ has been re-
265 assigned to the ν_5 C–C stretch mode, consistent with the propargyl cation retaining C_{2v}
266 symmetry in the excited state.

267 Hopefully, the current work will encourage measurement of the electronic spectrum for
268 bare $H_2C_3H^+$ in the gas phase. A single Ne atom should be a benign tag having little
269 effect on the electronic absorptions of the propargyl cation and it would be surprising if
270 the transitions of the bare $H_2C_3H^+$ molecule were displaced by more than 50 cm^{-1} from
271 those of $H_2C_3H^+$ -Ne. The current work also establishes foundations for IR-UV hole-burning
272 experiments to help disentangle the rather complicated $C_3H_3^+$ - N_2 IR spectrum which has
273 been postulated to include bands from several isomers in which N_2 is attached to $H_2C_3H^+$ and
274 $c\text{-}C_3H_3^+$ at different sites.

275 ACKNOWLEDGMENTS

276 This research was supported under the Australian Research Council’s Discovery Project
277 funding scheme (Project Numbers DP110100312 and DP120100100). The computations
278 were undertaken using resources provided by the NCI National Facility through the National
279 Computational Merit Allocation Scheme supported by the Australian Government, and
280 resources provided by the Victorian Life Sciences Computation Initiative. We would like to
281 thank J. F. Stanton (University of Texas, Austin) for helpful discussions on the convergence
282 of EOM methods with excitation level and for providing access to features not yet in the
283 released version of CFOUR.

284 REFERENCES

- 285 ¹F. P. Lossing, *Can. J. Chem.* **50**, 3973 (1972).
286 ²M. J. McEwan, C. L. McConnell, C. G. Freeman, and V. G. Anicich, *J. Phys. Chem.* **98**,
287 5068 (1994).
288 ³J. M. Goodings, D. K. Bohme, and N. Chun-Wai, *Combust. Flame* **36**, 27 (1979).
289 ⁴J. H. Waite Jr., You, T. E. Cravens, A. J. Coates, F. J. Crary, B. Magee, and J. Westlake,
290 *Science* **316**, 870 (2007).

- 291 ⁵A. Korth, M. L. Marconi, D. A. Mendis, F. R. Krueger, A. K. Richter, R. P. Lin, D. L.
292 Mitchell, K. A. Anderson, C. W. Carlson, H. Reme, J. A. Sauvaud, and C. d’Uston,
293 *Nature* **337**, 53 (1989).
- 294 ⁶E. Herbst, N. G. Adams, and D. Smith, *Astrophys. J.* **269**, 329 (1983).
- 295 ⁷P. Thaddeus, J. M. Vrtilik, and C. A. Gottlieb, *Astrophys. J.* **299**, L63 (1985).
- 296 ⁸P. Botschwina, R. Oswald, and G. Rauhut, *Phys. Chem. Chem. Phys.* **13**, 7921 (2011).
- 297 ⁹P. Botschwina, R. Oswald, and O. Dopfer, *Phys. Chem. Chem. Phys.* **13**, 14163 (2011).
- 298 ¹⁰X. Huang, P. R. Taylor, and T. J. Lee, *J. Phys. Chem. A* **115**, 5005 (2011).
- 299 ¹¹Z. Pachuau, K. S. Kharnaior, and R. H. D. Lyngdoh, *J. Chem. Sci.* **125**, 365 (2013).
- 300 ¹²D. W. Minsek and P. Chen, *J. Phys. Chem.* **94**, 8399 (1990).
- 301 ¹³H. Gao, Z. Lu, L. Yang, Z. J., and C. Y. Ng, *J. Chem. Phys.* **137**, 161101 (2012).
- 302 ¹⁴O. Dopfer, D. Roth, and J. P. Maier, *Int. J. Mass Spectrom.* **218**, 281 (2002).
- 303 ¹⁵A. M. Ricks, G. E. Douberly, P. v. R. Schleyer, and M. A. Duncan, *J. Chem. Phys.* **132**,
304 0511011 (2010).
- 305 ¹⁶M. Wyss, E. Riaplov, and J. P. Maier, *J. Chem. Phys.* **114**, 10355 (2001).
- 306 ¹⁷M. A. Duncan, *J. Phys. Chem. A* **116**, 11477 (2012).
- 307 ¹⁸D. A. Wild and E. J. Bieske, *Int. Rev. Phys. Chem.* **22**, 129 (2003).
- 308 ¹⁹V. Dryza, N. Chalyavi, J. Sanelli, and E. Bieske, *J. Chem. Phys.* **137**, 204304 (2012).
- 309 ²⁰V. Dryza, J. A. Sanelli, E. G. Robertson, and E. J. Bieske, *J. Phys. Chem. A* **116**, 4323
310 (2012).
- 311 ²¹N. Chalyavi, V. Dryza, J. A. Sanelli, and E. J. Bieske, *J. Chem. Phys.* **138**, 224307 (2013).
- 312 ²²J. Olsen, B. O. Roos, P. Jørgensen, and H. J. A. Jensen, *J. Chem. Phys.* **89**, 2185 (1988).
- 313 ²³K. Aidas, C. Angeli, K. L. Bak, V. Bakken, R. Bast, L. Boman, O. Christiansen, R. Cimi-
314 raglia, S. Coriani, P. Dahle, E. K. Dalskov, U. Ekström, T. Enevoldsen, J. J. Eriksen,
315 P. Ettenhuber, B. Fernández, L. Ferrighi, H. Fliegl, L. Frediani, K. Hald, A. Halkier,
316 C. Hättig, H. Heiberg, T. Helgaker, A. C. Hennum, H. Hettema, E. Hjertenæs, S. Høst, I.-
317 M. Høyvik, M. F. Iozzi, B. Jansík, H. J. Aa. Jensen, D. Jonsson, P. Jørgensen, J. Kauczor,
318 S. Kirpekar, T. Kjærgaard, W. Klopper, S. Knecht, R. Kobayashi, H. Koch, J. Kongsted,
319 A. Krapp, K. Kristensen, A. Ligabue, O. B. Lutnæs, J. I. Melo, K. V. Mikkelsen, R. H.
320 Myhre, C. Neiss, C. B. Nielsen, P. Norman, J. Olsen, J. M. H. Olsen, A. Osted, M. J.
321 Packer, F. Pawłowski, T. B. Pedersen, P. F. Provasi, S. Reine, Z. Rinkevicius, T. A. Ruden,
322 K. Ruud, V. V. Rybkin, P. Salek, C. C. M. Samson, A. S. de Merás, T. Saue, S. P. A.

323 Sauer, B. Schimmelpfennig, K. Snekskov, A. H. Steindal, K. O. Sylvester-Hvid, P. R. Tay-
324 lor, A. M. Teale, E. I. Tellgren, D. P. Tew, A. J. Thorvaldsen, L. Thøgersen, O. Vahtras,
325 M. A. Watson, D. J. D. Wilson, M. Ziolkowski, and H. Ågren, *WIREs Comput. Mol. Sci.*
326 **4**, 269 (2014).

327 ²⁴CFOUR, a quantum chemical program package written by J.F. Stanton, J. Gauss, M.E.
328 Harding, P.G. Szalay with contributions from A.A. Auer, R.J. Bartlett, U. Benedikt, C.
329 Berger, D.E. Bernholdt, Y.J. Bomble, L. Cheng, O. Christiansen, M. Heckert, O. Heun, C.
330 Huber, T.-C. Jagau, D. Jonsson, J. Jusélius, K. Klein, W.J. Lauderdale, D.A. Matthews,
331 T. Metzroth, L.A. Mück, D.P. O’Neill, D.R. Price, E. Prochnow, C. Puzzarini, K. Ruud,
332 F. Schiffmann, W. Schwalbach, C. Simmons, S. Stopkowicz, A. Tajti, J. Vázquez, F.
333 Wang, J.D. Watts and the integral packages MOLECULE (J. Almlöf and P.R. Taylor),
334 PROPS (P.R. Taylor), ABACUS (T. Helgaker, H.J. Aa. Jensen, P. Jørgensen, and J.
335 Olsen), and ECP routines by A. V. Mitin and C. van Wüllen. For the current version, see
336 <http://www.cfour.de>.

337 ²⁵R. S. Mulliken, *J. Chem. Phys.* **23**, 1997 (1955).

338 ²⁶J. D. Chai and M. Head-Gordon, *Phys. Chem. Chem. Phys.* **10**, 6615 (2008).

339 ²⁷N. Chalyavi, K. J. Catani, J. A. Sanelli, V. Dryza, and E. J. Bieske, *Mol. Phys.* **113**, 2086
340 (2015).

341 ²⁸M. J. Frisch, G. W. Trucks, H. B. Schlegel, G. E. Scuseria, M. A. Robb, J. R. Cheese-
342 man, G. Scalmani, V. Barone, B. Mennucci, G. A. Petersson, H. Nakatsuji, M. Caricato,
343 X. Li, H. P. Hratchian, A. F. Izmaylov, J. Bloino, G. Zheng, J. L. Sonnenberg, M. Hada,
344 M. Ehara, K. Toyota, R. Fukuda, J. Hasegawa, M. Ishida, T. Nakajima, Y. Honda, O. Ki-
345 tao, H. Nakai, T. Vreven, J. A. Montgomery, Jr., J. E. Peralta, F. Ogliaro, M. Bearpark,
346 J. J. Heyd, E. Brothers, K. N. Kudin, V. N. Staroverov, R. Kobayashi, J. Normand,
347 K. Raghavachari, A. Rendell, J. C. Burant, S. S. Iyengar, J. Tomasi, M. Cossi, N. Rega,
348 J. M. Millam, M. Klene, J. E. Knox, J. B. Cross, V. Bakken, C. Adamo, J. Jaramillo,
349 R. Gomperts, R. E. Stratmann, O. Yazyev, A. J. Austin, R. Cammi, C. Pomelli, J. W.
350 Ochterski, R. L. Martin, K. Morokuma, V. G. Zakrzewski, G. A. Voth, P. Salvador,
351 J. J. Dannenberg, S. Dapprich, A. D. Daniels, Ö. Farkas, J. B. Foresman, J. V. Ortiz,
352 J. Cioslowski, and D. J. Fox, “Gaussian 09 Revision A.1,” Gaussian Inc. Wallingford CT
353 2009.

354 ²⁹See supplemental material at [URL will be inserted by AIP] for a compilation of calculated

355 vibrational frequencies for $\text{H}_2\text{C}_3\text{H}^+$, $\text{H}_2\text{C}_3\text{H}^+\text{-Ne}$ and $\text{H}_2\text{C}_3\text{H}^+\text{-N}_2$, fully assigned spectra of
356 $\text{H}_2\text{C}_3\text{H}^+\text{-Ne}$ and $\text{H}_2\text{C}_3\text{H}^+\text{-N}_2$, and simulated spectra of $\text{H}_2\text{C}_3\text{H}^+$.

TABLE III. Measured transition frequencies and assignments for the $\tilde{A}^1A_1 \leftarrow \tilde{X}^1A_1$ band system of $\text{H}_2\text{C}_3\text{H}^+-\text{N}_2$ and $\text{H}_2\text{C}_3\text{H}^+-\text{Ne}$.

Assignment	$\text{H}_2\text{C}_3\text{H}^+-\text{N}_2$		$\text{H}_2\text{C}_3\text{H}^+-\text{Ne}$	
	$\tilde{\nu}$	$\Delta\tilde{\nu}$	$\tilde{\nu}$	$\Delta\tilde{\nu}$
0_0^0 iso 2	37569	-134	-	-
0_0^0	37703	0	37618	0
s_0^1	37797	95	-	-
s_0^2	37890	187	-	-
5_0^1 iso 2	38204	501	-	-
5_0^1	38334	631	38251	633
$5_0^1 s_0^1$	38432	729	-	-
$5_0^1 s_0^2$	38521	818	-	-
5_0^2 iso 2	38844	1141	-	-
5_0^2	38965	1262	38875	1257
4_0^1	-	-	38965	1346
$5_0^2 s_0^1$	39056	1353	-	-
$5_0^2 s_0^2$	39148	1445	-	-
6_0^2	39279	1576	39204	1585
5_0^3 iso 2	39467	1764	-	-
5_0^3	39596	1893	39500	1881
$4_0^1 5_0^1$	-	-	39583	1965
$5_0^3 s_0^1$	39680	1977	-	-
$5_0^3 s_0^2$	39781	2078	-	-
$5_0^1 6_0^2$	39895	2192	39824	2206
5_0^4 iso 2	40089	2386	-	-
5_0^4	40230	2527	40133	2514
$4_0^1 5_0^2$	-	-	40195	2577
$5_0^4 s_0^1$	40302	2599	-	-
$5_0^4 s_0^2$	40388	2685	-	-
$5_0^2 6_0^2$	40514	2811	40433	2815
2_0^1*	40600	2897	40530	2912
$5_0^5/6_0^4$	40876	3173	40777	3158
$5_0^3 6_0^2$	41159	3456	41071	3452
$2_0^1 5_0^1*$	41231	3528	41127	3508
5_0^6	41529	3826	41470	3851
$5_0^4 6_0^2/2_0^1 5_0^2*$	41823	4120	41734	4115
5_0^7	42189	4486	42085	4467

* tentative assignment